International Journal of Solids and Structures 51 (2014) 3113–3118

Contents lists available at ScienceDirect

International Journal of Solids and Structures

journal homepage: www.elsevier.com/locate/ijsolstr

Buckling of a stiff thin film on a pre-strained bi-layer substrate

Huanyu Cheng [a], Yihui Zhang [a,b,*], Keh-Chih Hwang [b], John A. Rogers [c], Yonggang Huang [a,*]

[a] Departments of Mechanical Engineering and Civil and Environmental Engineering, Center for Engineering and Health, and Skin Disease Research Center, Northwestern University, Evanston, IL 60208, USA
[b] Center for Mechanics and Materials, Tsinghua University, Beijing 100084, China
[c] Department of Materials Science and Engineering, University of Illinois, Urbana, IL 61801, USA

ARTICLE INFO

Article history:
Received 26 February 2014
Received in revised form 6 April 2014
Available online 21 May 2014

Keywords:
Pre-strain
Bi-layer substrate
Buckling analysis
Stretchable electronics

ABSTRACT

Controlled buckling can impart stretchable mechanics to brittle materials when integrated as thin films on soft, elastomeric substrates. Typical elastomers are permeable to fluids, however, and therefor unable to provide robust barriers to entry of water, for instance, into devices built with the supported thin films. In addition, the mechanical strength of a system dominated by a soft substrate is often unsatisfactory for realistic applications. We show that introduction of a bi-layer substrate yields a robust, high strength system that maintains stretchable characteristics, with a soft layer on top of a relatively stiff layer in the substrate. As a mechanical protection, a soft encapsulation layer can be used on top of the device and the stretchability of the encapsulated system is smaller than that of the system without encapsulation. A simple, analytic model, validated by numerical analysis and FEA, is established for stiff thin films on a bi-layer substrate, and is useful to the design of stretchable systems.

Published by Elsevier Ltd.

1. Introduction

With the ability to conform to biological tissues and monitor vital physiological signals, stretchable electronics (Song et al., 2014; Lu et al., 2012; Kim et al., 2011a) have the potential to provide a promising platform for biomedical devices as diagnostics and/or therapeutics for clinical purposes (Kim et al., 2011b; Jeong et al., 2013; Webb et al., 2013). Controlled buckling realized by the pre-strain strategy (Jiang et al., 2007; Huang et al., 2005; Allen, 1969; Song et al., 2008; Wang and Zhao, 2014; Zang et al., 2013; Cao et al., 2013; Lu et al., 2007) can generate sophisticated micro- and nano-structures in stretchable electronics (Kim et al., 2011b; Ko et al., 2008; Xiao et al., 2010; Xiao et al., 2009; Duan et al., 2013). Here, as shown in Fig. 1, a stiff film is first transfer printed (Yang et al., 2012; Kim et al., 2012; Cheng et al., 2012) onto a flat, pre-strained elastomeric substrate. When the elastomer returns to its original length upon release of the pre-strain, the film buckles into a wavy geometry, which affords, then, an effective level of stretchable mechanics. With x and z in the film length and thickness directions (Fig. 1a), the out-of-plane displacement w_0 of the buckled thin film can be represented by a sinusoidal function $w_0 = A\cos(kx)$, where A and k are the characteristic amplitude and wave number to be determined. With the film thickness h_f much smaller than the buckle wavelength $2\pi/k$, the thin film is modeled as a beam. Jiang et al. (2007) studied the buckling and post-buckling behaviors of thin film on a single-layer substrate. The total energy of the buckled system consists of bending energy and membrane energy of the film, and elastic energy of the substrate. The bending energy U_b and membrane energy U_m, which will be used in the present study, are given analytically as (Jiang et al., 2007)

$$U_b = \frac{k^4 \bar{E}_f h_f^3 A^2}{48(1+\varepsilon_{pre})^4} L, \quad U_m = \frac{\bar{E}_f h_f}{2}\left[\frac{k^2 A^2}{4(1+\varepsilon_{pre})^2} - \frac{\varepsilon_{pre}}{1+\varepsilon_{pre}}\right]^2 L, \qquad (1)$$

where ε_{pre} is the pre-strain applied to the substrate, $\bar{E}_f$ is the plane-strain modulus of the thin film, and L is the film length at the original, unstretched state (Fig. 1b).

The soft substrate plays a key role in the pre-strain strategy. However, being permeable to fluids, the single-layer soft substrate cannot encapsulate the device well, and it is also difficult to integrate with liquid components (Xu et al., 2013). Furthermore, electronics built on unusual substrates, ranging from fabrics to plastic sheets, have great potential for use in biomedical devices (Kim et al., 2009). To enable a stretchable capability in integrated electronics, another soft layer is introduced on top of such unusual types of substrates, resulting in a bi-layer structure, where the soft

* Corresponding authors at: Departments of Mechanical Engineering and Civil and Environmental Engineering, Center for Engineering and Health, and Skin Disease Research Center, Northwestern University, Evanston, IL 60208, USA. Tel.: +1 847 467 3165 (Y. Huang).

E-mail addresses: yihui.zhang@northwestern.edu (Y. Zhang), y-huang@northwestern.edu (Y. Huang).

http://dx.doi.org/10.1016/j.ijsolstr.2014.05.012
0020-7683/Published by Elsevier Ltd.

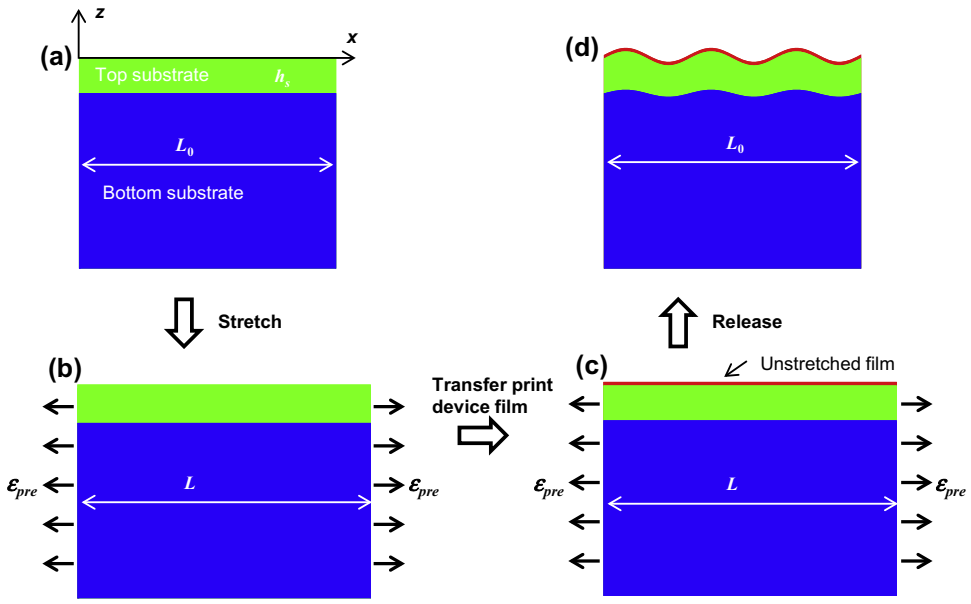

Fig. 1. Schematic illustration of a buckled stiff thin film on a bi-layer substrate.

layer on top facilitates buckling of thin films and the relatively stiff layer at the bottom can significantly enhance the strength of the system (Kim et al., 2009). Careful choice of the bottom layer can further improve the robustness, providing chemical and thermal resistances to the system (García et al., 2010). This bi-layer substrate design is not only critical for use in stretchable electronics, but it can also create opportunities such as integration with liquid components or enhanced strength and robustness in classes of electronics built to dissolve completely after function in the human body or environment via resorption, thereby eliminating the need for recollection (Hwang et al., 2012; Li et al., 2013). To understand the system with a bi-layer substrate, we perform analytic study on buckling and post-buckling behaviors. The elastic energy of the bi-layer substrate is obtained in Section 2. The energy method is then used to study the buckling and postbuckling in Sections 3 and 4, respectively.

2. Elastic energy of bi-layer substrate

Fig. 1 illustrates the pre-strain strategy where a stiff thin film buckles on a bi-layer substrate. The top substrate layer is usually much thicker than the thin film, i.e., its thickness $h_s \gg h_f$ (e.g., $h_s = 1$ mm and $h_f = 100$ μm as in experiments). The bottom substrate layer is much thicker than the top layer (e.g., 10 times) Kim et al., 2009, and is therefore modeled as a semi-infinite solid. Similar to thin film buckling on a single-layer substrate, the out-of-plane displacement of buckled thin film on a bi-layer substrate can also be represented by a sinusoidal function $w_0 = A\cos(kx)$. In the system of a stiff thin film buckled on a pre-strained, single-layer substrate, Song et al. (2008) developed a finite deformation theory, which explains the buckled amplitude and wavelength very well. Cheng and Song (2013) further showed that finite geometry change of the thin film dominates in the finite deformation theory, which was also confirmed to apply for the bi-layer substrate in the finite element analysis (FEA). In FEA, a Mooney–Rivlin hyperelastic model was used for both the top and bottom substrate layers. The results were compared with those obtained using linear elastic model, which only shows a slight difference. Therefore, linear elastic model is used in the following analytic study for the bi-layer substrate.

Let u_i and w_i denote the displacements in the x and z directions (Fig. 1a), with $i = 1, 2$ representing the top and bottom layers of the substrate, respectively. The equilibrium equations can be written in terms of the displacements as (Timoshenko and Goodier, 2011)

$$\begin{aligned}&\left(\frac{\partial^2 u_i}{\partial x^2}+\frac{\partial^2 u_i}{\partial z^2}\right)+\frac{1}{1-2\nu_i}\frac{\partial}{\partial x}\left(\frac{\partial u_i}{\partial x}+\frac{\partial w_i}{\partial z}\right)=0,\\&\left(\frac{\partial^2 w_i}{\partial x^2}+\frac{\partial^2 w_i}{\partial z^2}\right)+\frac{1}{1-2\nu_i}\frac{\partial}{\partial z}\left(\frac{\partial u_i}{\partial x}+\frac{\partial w_i}{\partial z}\right)=0,\end{aligned} \tag{2}$$

where ν_i is the Poisson's ratio of each substrate layer. Let $z = 0$ denote the top surface of the substrate. Continuity of displacement between the thin film and substrate requires

$$w_1|_{z=0} = w_0 = A\cos(kx). \tag{3}$$

The shear at the film/substrate interface is negligible (Huang et al., 2005) because the thin film is much stiffer than both substrate layers (Kim et al., 2009), which gives

$$\left(\frac{\partial u_1}{\partial z}+\frac{\partial w_1}{\partial x}\right)\Big|_{z=0} = 0. \tag{4}$$

Continuity of displacement and stress requires

$$\begin{aligned}&u_1|_{z=-h_s} = u_2|_{z=-h_s}, \quad w_1|_{z=-h_s} = w_2|_{z=-h_s},\\&\sigma_{z1}|_{z=-h_s} = \sigma_{z2}|_{z=-h_s}, \quad \tau_1|_{z=-h_s} = \tau_2|_{z=-h_s},\end{aligned} \tag{5}$$

where σ_z and τ are the normal and shear stresses.

The displacement field can be expressed as $(u_i, w_i) = [U_i(z)\sin(kx), W_i(z)\cos(kx)]$. Its substitution into Eq. (2) gives the solution

$$\begin{aligned}&U_1 = C_1 e^{kz} + C_2 e^{-kz} + C_3 z e^{kz} + C_4 z e^{-kz},\\&W_1 = -C_1 e^{kz} + C_2 e^{-kz} + \left(\frac{3-4\nu_i}{k} - z\right)C_3 e^{kz} + \left(\frac{3-4\nu_i}{k} + z\right)C_4 e^{-kz},\end{aligned} \tag{6a}$$

$$\begin{aligned}&U_2 = C_5 e^{kz} + C_6 z e^{kz},\\&W_2 = -C_5 e^{kz} + \left(\frac{3-4\nu_i}{k} - z\right)C_6 e^{kz},\end{aligned} \tag{6b}$$

where the constants C_j $(j = 1, \ldots, 6)$ are to be determined from the six linear algebraic equations resulting from the boundary and continuity conditions (3)–(5), and they are all linearly proportional to A.

The elastic energy of the bi-layer substrate is then obtained as

$$U_s = \frac{1}{4}\bar{E}_{s1} g k A^2 L_0, \tag{7}$$

where L_0 is the substrate length at the original, unstretched state (Fig. 1a) and is related to the film length L at its original, unstretched state by $L = L_0(1+\varepsilon_{pre})$; $\bar{E}_{s1} = E_{s1}/(1-\nu_1^2)$ is the plane-strain modulus of top substrate layer, and

$$g = \frac{1-\nu_1}{kA}[-k(C_1+C_2) + 2(1-\nu_1)(C_3-C_4)], \tag{8}$$

is independent of A. For an incompressible substrate $\nu_1 = \nu_2 = 0.5$ as in experiments (Kim et al., 2009), g is given as

$$g = g(\eta) = \frac{1}{2}\frac{(1+r^2)\cosh(\eta) + 2r\sinh(\eta) + \left(1+\frac{\eta^2}{2}\right)(1-r^2)}{(1+r^2)\sinh(\eta) + 2r\cosh(\eta) - \eta(1-r^2)}, \tag{9}$$

where $r = E_{s1}/E_{s2}$ is the ratio of Young's moduli of the top to bottom substrate layers, and $\eta = 2kh_s$ is the non-dimensional wave number, which represents the ratio of the thickness of the top substrate layer to the wavelength. For the limit of top and bottom substrate layers having the same modulus ($r = 1$) or the limit of a very thick top layer ($h_s \to \infty$), g approaches 1/2, corresponding to that for a thick single-layer substrate (Jiang et al., 2007). For the top substrate layer much more compliant than the bottom layer (i.e., $r \ll 1$) Kim et al., 2009 and its thickness larger than one half of the wavelength (i.e., $\eta > 2\pi$), Eq. (9) can be simplified, within 0.2% error, to

$$g \approx \frac{1}{2}\left(1 + \frac{2+2\eta+\eta^2}{1+2r}e^{-\eta}\right). \tag{9a}$$

3. Buckling analysis of stiff films on bi-layer substrate

The total energy of the buckled thin film on a bi-layer substrate consists of bending energy U_b and membrane energy U_m of the film given in Eq. (1) and the elastic energy of the substrate U_s in Eq. (7), i.e., $U_{total} = U_b + U_m + U_s$. Minimization of the total energy $\partial U_{tot}/\partial A = \partial U_{tot}/\partial k = 0$ gives the following equation for the wave number k,

$$\frac{\bar{E}_f h_f^3}{6\bar{E}_{s1}(1+\varepsilon_{pre})^3}k^3 = g - k\frac{dg}{dk}, \tag{10}$$

whereas the amplitude A is given by

$$A = \sqrt{\frac{4}{k^2}\varepsilon_{pre}(1+\varepsilon_{pre}) - \frac{4\bar{E}_{s1}}{\bar{E}_f h_f k^3}g(1+\varepsilon_{pre})^3 - \frac{h_f^2}{3}}. \tag{11}$$

Substitution of Eq. (9a) into Eq. (10) gives

$$\frac{1}{24(1+\varepsilon_{pre})^3}\frac{\bar{E}_f h_f^3}{\bar{E}_{s1} h_s^3}\eta^3 = 1 + \frac{2+2\eta+\eta^2+\eta^3}{1+2r}e^{-\eta}. \tag{12}$$

For the limit of a single-layer substrate ($h_s \to \infty$), the second term on the right hand side $(2+2\eta+\eta^2+\eta^3)e^{-\eta}/(1+2r)$ vanishes, and η has the solution

$$\eta_0 = 4(1+\varepsilon_{pre})\sqrt{\varepsilon_c}\frac{h_s}{h_f}, \tag{13}$$

where $\varepsilon_c = (3\bar{E}_{s1}/\bar{E}_f)^{2/3}/4$ is the critical buckling strain for the thin film buckled on a single-layer substrate (Jiang et al., 2007), which is very small for stiff films on a compliant substrate [e.g., $\varepsilon_c = 0.034\%$ for the Si films (Young's modulus of 130 GPa) on PDMS substrate (Young's modulus of 1.8 MPa)] (Jiang et al., 2007). For a top layer with finite thickness h_s, η can be expressed as $\eta = \eta_0(1+\Delta)$, where Δ can be solved from Eq. (12) by the method of perturbation as $\Delta = \eta_0^3 e^{-\eta_0}/[3(1+2r)]$ for $\Delta \ll 1$. (For example, $\Delta < 0.15$ for $\eta_0 = 2\pi$.) This gives

$$\eta = \eta_0\left[1 + \frac{\eta_0^3}{3(1+2r)}e^{-\eta_0}\right], \tag{14}$$

or equivalently in terms of the wave number k and wavelength λ as

$$k = \frac{2(1+\varepsilon_{pre})\sqrt{\varepsilon_c}}{h_f}\left[1 + \frac{\eta_0^3}{3(1+2r)}e^{-\eta_0}\right],$$
$$\lambda = \frac{\pi h_f}{(1+\varepsilon_{pre})\sqrt{\varepsilon_c}}\frac{1}{1+\frac{\eta_0^3}{3(1+2r)}e^{-\eta_0}}. \tag{14a}$$

Its substitution into Eq. (11) gives the amplitude

$$A = \frac{h_f}{1+\frac{\eta_0^3}{3(1+2r)}e^{-\eta_0}}\sqrt{\frac{\varepsilon_{pre}}{(1+\varepsilon_{pre})\varepsilon_c} - 1}$$
$$\approx \frac{h_f}{1+\frac{\eta_0^3}{3(1+2r)}e^{-\eta_0}}\sqrt{\frac{\varepsilon_{pre}}{(1+\varepsilon_{pre})\varepsilon_c}}, \tag{15}$$

where the last approximation holds for the pre-strain $\varepsilon_{pre} \gg \varepsilon_c$. The buckle amplitude vanishes once the pre-strain reaches $\varepsilon_c/(1-\varepsilon_c)$, which is very small and approximately equals ε_c. Once the film buckles, the membrane strain at the midpoint of the film thickness remains a very small constant, $-\varepsilon_c$. Therefore the maximum strain in the film, which determines the stretchability of the system, is dominated by the bending strain and is given by

$$\varepsilon_{\max} \approx 2\left[1 + \frac{\eta_0^3}{3(1+2r)}e^{-\eta_0}\right]\sqrt{\frac{\varepsilon_{pre}\varepsilon_c}{1+\varepsilon_{pre}}}. \tag{16}$$

Eqs. (14)–(16) all indicate the effect of the bottom substrate layer is only through the modulus ratio r in the term $\eta_0^3 e^{-\eta_0}/[3(1+2r)]$, which is less than 15% for $\eta_0 \geqslant 2\pi$. Therefore, the Young's modulus (and thickness) of top substrate layer dominates over that of bottom substrate layer in determining the wavelength, amplitude and maximum strain of the buckled film.

Fig. 2 compares the wavelength in Eq. (14a) and amplitude in Eq. (15) to the numerical solution of Eqs. (10) and (11), respectively, in order to validate the perturbation method used. Here the wavelength and amplitude are normalized by their counterparts $\lambda_{singlelayer} = \pi h_f/[(1+\varepsilon_{pre})\sqrt{\varepsilon_c}]$ and $A_{singlelayer} = h_f\sqrt{\varepsilon_{pre}/[(1+\varepsilon_{pre})\varepsilon_c]}$ for a thick, single-layer substrate (Cheng and Song, 2013). The normalized wavelength and amplitude have the same expression $\lambda/\lambda_{singlelayer} = A/A_{singlelayer} = \{1+\eta_0^3 e^{-\eta_0}/[3(1+2r)]\}^{-1}$. Fig. 2a shows the normalized wavelength and amplitude decrease as the ratio of Young's moduli r decreases, and become independent of r for $r \leqslant 1/20$. Therefore, r is fixed at 1/20 in the following analysis. Within 13% error from the accurate but numerical solution of Eqs. (10) and (11) for $\eta_0 > 2\pi$ (Fig. 2b), this simple, normalized solution is useful in the experimental design. Finite Element Analysis was also used to validate the above analysis for silicon thin films (Young's modulus $E_f = 130$ GPa, Poisson's ratio 0.27, and film thickness ranging from 100 to 500 nm) on the top substrate layer of Silbione ($E_{s1} = 10$ kPa, thickness 100 μm) and bottom substrate layer of fabric ($E_{s2} = 400$ kPa). The thin film and bi-layer substrate were modeled by the beam elements (B21 in the ABAQUS ABAQUS, 2009 finite element program) and the 4-node plane strain elements (CPE4R in ABAQUS), respectively. Element mesh was refined to ensure the convergence of the results. The length of the two-dimensional system is 2.5 mm and it is much larger than the wavelength of the buckled system. To avoid the edge effect, both wavelength and amplitude were measured in the middle region

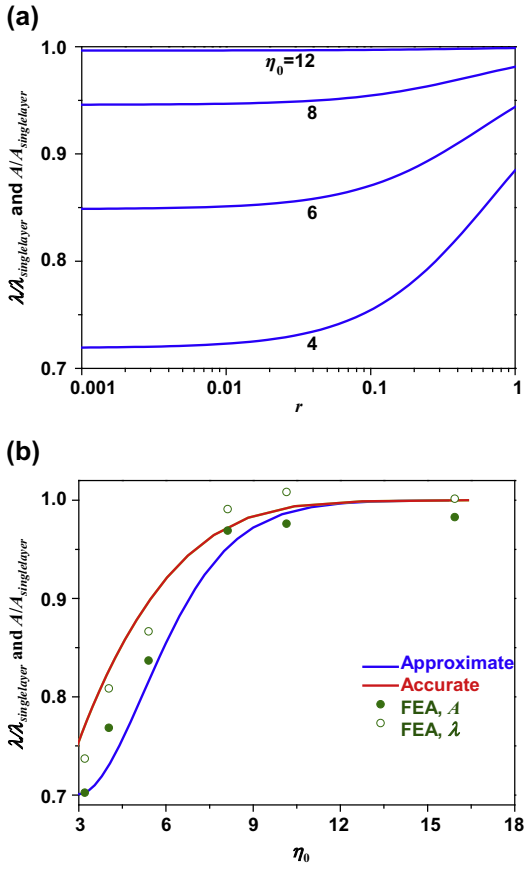

Fig. 2. Normalized wavelength $\lambda/\lambda_{singlelayer}$ and amplitude $A/A_{singlelayer}$ versus (a) the moduli ratio r of top to bottom substrate layers for different η_0 values and (b) η_0 for $r = 1/20$.

where a uniform sinusoidal shape was observed. The FEA result is in a good agreement with both the numerical solution and the normalized function. For a pre-strain of 25% applied on a relative thick substrate layer where the thickness of fabric is five times of that of Silbione, the amplitude 13.01 μm and wavelength 78.17 μm of the buckled film obtained by FEA are in excellent agreement with 13.33 and 77.02 μm from Eqs. (14a) and (15). As shown in Fig. 2b, the solution of bi-layer substrate approaches that of the single layer substrate for $\eta_0 > 10$ (within 1% error), which indicates that the effect of stiffer bottom substrate is negligible if the top substrate layer is thicker than 80% of the wavelength for a single layer substrate, $h_s > 0.8\lambda_{singlelayer}$, or equivalently $h_s > 5[\bar{E}_f/(3\bar{E}_{s1})]^{1/3}h_f$. Fig. 3 shows the maximum strain in the film from Eq. (16), normalized by its counterpart $2\sqrt{\varepsilon_{pre}\varepsilon_c/(1+\varepsilon_{pre})}$ for a thick, single-layer substrate, versus η_0. The relative error between the maximum strain in Eq. (16) and the numerical solution from Eqs. (10) and (11) is <1% for $\eta_0 > 9.3$, and is <6.6% for $\eta_0 > 2\pi$.

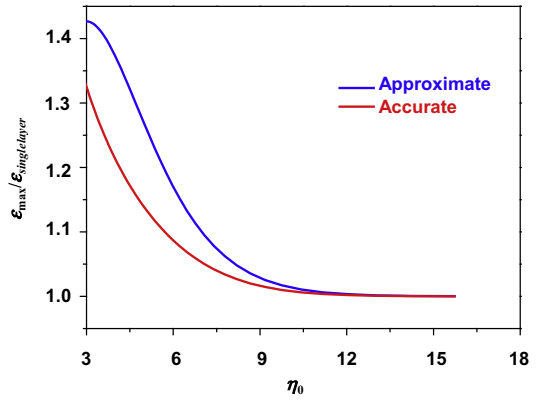

Fig. 3. Maximum strain ε_{max} normalized by its counterpart $2\sqrt{\varepsilon_{pre}\varepsilon_c/(1+\varepsilon_{pre})}$ for a thick, single-layer substrate versus η_0 for $r = 1/20$.

4. Encapsulation and post-buckling analysis

An encapsulation layer is casted and cured on top of the unbuckled film to provide mechanical protection in the experiment as shown in Fig. 4a (Fan et al., 2014). After the release of the pre-strain, the encapsulation layer buckles with the film (Fig. 4b), which changes the morphology of buckled film from that in Section 3, and the morphology also changes when the encapsulated system is stretched (Fig. 4c). For an applied strain ε_{appl} shown in Fig. 4c, the wavy morphology can be determined following the same approach as in Section 3 by accounting for the elastic energy in the encapsulation layer.

The out-of-plane displacement of the film can also be represented by a sinusoidal function $w_{stretch} = \tilde{A}\cos(\tilde{k}\tilde{x})$ with the characteristic amplitude $\tilde{A}$ and wave number $\tilde{k}$, where $\tilde{x} = x(1+\varepsilon_{appl})$ is the coordinate at the stretched state. These give the displacement at the original, unstretched state as $w_{stretch} = \tilde{A}\cos[\tilde{k}(1+\varepsilon_{appl})x]$. The bending and membrane energies become (Cheng and Song, 2013)

$$\tilde{U}_b = \frac{\tilde{k}^4\bar{E}_f h_f^3\tilde{A}^2(1+\varepsilon_{appl})^4}{48(1+\varepsilon_{pre})^4}L,$$

$$\tilde{U}_m = \frac{\bar{E}_f h_f}{2}\left[\frac{\tilde{k}^2\tilde{A}^2(1+\varepsilon_{appl})^2}{4(1+\varepsilon_{pre})^2} + \frac{\varepsilon_{appl}-\varepsilon_{pre}}{1+\varepsilon_{pre}}\right]^2 L, \tag{17}$$

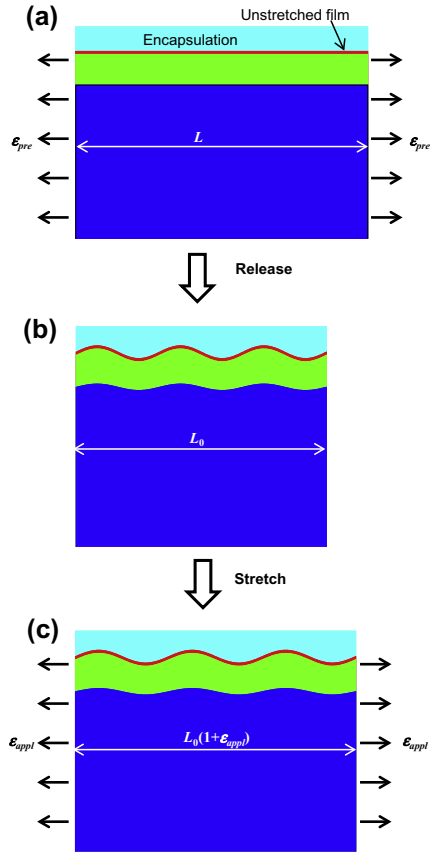

Fig. 4. Schematic illustration of the buckled system with encapsulation layer.

which degenerate to Eq. (1) for $\varepsilon_{appl}=0$. Subject to a normal displacement of $w_{stretch}$ on the top surface of substrate, the elastic energy of the bi-layer substrate becomes $\tilde{U}_s=\bar{E}_{s1}g\tilde{k}\tilde{A}^2L_0(1+\varepsilon_{appl})/4$, with replacing k and A with $\tilde{k}(1+\varepsilon_{appl})$ and $\tilde{A}$ in Eq. (7), respectively, where g is given in Eq. (9). The original, unstretched state for the encapsulation is the same as that for the film, therefore, the out-of-plane displacement $w_{stretch}$ can be rewritten as $w_{stretch}=\tilde{A}\cos[\bar{x}\tilde{k}(1+\varepsilon_{appl})/(1+\varepsilon_{pre})]$, where $\bar{x}$ is the coordinate at the original, unstretched state for the encapsulation. For a pre-strain of ε_{pre} applied on the bi-layer substrate, the strain applied on the encapsulation is simply $-\varepsilon_{pre}/(1+\varepsilon_{pre})$ when the pre-strain is released. The magnitude of this compressive strain is smaller than the pre-strain such that the linear elastic model is used for the encapsulation, just as the linear elastic model for the bi-layer substrate. For a thick encapsulation layer with the plane-strain modulus $\bar{E}_e$, its elastic energy can be obtained by replacing k and L_0 with $\tilde{k}(1+\varepsilon_{appl})/(1+\varepsilon_{pre})$ and $L_0(1+\varepsilon_{pre})$ in Eq. (7), which gives $\tilde{U}_e=\bar{E}_e\tilde{k}\tilde{A}^2L_0(1+\varepsilon_{appl})/8$. Minimization of the total energy $\tilde{U}_{total}$ $(=\tilde{U}_b+\tilde{U}_m+\tilde{U}_s+\tilde{U}_e)$ with respect to the wave number and amplitude gives

$$\frac{\bar{E}_f h_f^3(1+\varepsilon_{appl})^3}{6\bar{E}_{s1}(1+\varepsilon_{pre})^3}\tilde{k}^3=\frac{\bar{E}_e}{2\bar{E}_{s1}}+g-\tilde{k}\frac{dg}{d\tilde{k}},$$
$$\tilde{A}=\sqrt{\frac{4}{\tilde{k}^2}\frac{(\varepsilon_{pre}-\varepsilon_{appl})(1+\varepsilon_{pre})}{(1+\varepsilon_{appl})^2}-\frac{2(2\bar{E}_{s1}g+\bar{E}_e)(1+\varepsilon_{pre})^3}{\bar{E}_f h_f\tilde{k}^3(1+\varepsilon_{appl})^3}-\frac{h_f^2}{3}}. \tag{18}$$

Similar to Eq. (14), the normalized wave number $\tilde{\eta}=2h_s\tilde{k}$ can be solved by the perturbation method as $\tilde{\eta}=\tilde{\eta}_0(1+\tilde{\Delta})$, where

$$\tilde{\eta}_0=4\frac{1+\varepsilon_{pre}}{1+\varepsilon_{appl}}\sqrt{\varepsilon_c}\frac{h_s}{h_f}\left(1+\frac{\bar{E}_e}{\bar{E}_{s1}}\right)^{1/3}, \tag{19}$$

and $\tilde{\Delta}=\tilde{\eta}_0^3e^{-\tilde{\eta}_0}/[3(1+2r)(\bar{E}_{s1}+\bar{E}_e)/\bar{E}_{s1}]$. The wavelength $\tilde{\lambda}$ is subsequently obtained as

$$\tilde{\lambda}=\frac{2\pi}{\tilde{k}}=\frac{\pi h_f}{\sqrt{\varepsilon_c}}\frac{1+\varepsilon_{appl}}{1+\varepsilon_{pre}}\frac{1}{\left(1+\frac{\bar{E}_e}{\bar{E}_{s1}}\right)^{1/3}\left[1+\frac{\tilde{\eta}_0^3e^{-\tilde{\eta}_0}}{3(1+2r)\left(1+\frac{\bar{E}_e}{\bar{E}_{s1}}\right)}\right]}. \tag{20}$$

Its substitution into Eq. (18) gives the amplitude

$$\tilde{A}\approx\frac{h_f}{\left(1+\frac{\bar{E}_e}{\bar{E}_{s1}}\right)^{1/3}\left[1+\frac{\tilde{\eta}_0^3e^{-\tilde{\eta}_0}}{3(1+2r)\left(1+\frac{\bar{E}_e}{\bar{E}_{s1}}\right)}\right]}\sqrt{\frac{\varepsilon_{pre}-\varepsilon_{appl}}{(1+\varepsilon_{pre})\varepsilon_c}}. \tag{21}$$

The maximum strain in the thin film is then given by

$$\varepsilon_{\max}\approx 2\left(1+\frac{\bar{E}_e}{\bar{E}_{s1}}\right)^{1/3}\left[1+\frac{\tilde{\eta}_0^3e^{-\tilde{\eta}_0}}{3(1+2r)\left(1+\frac{\bar{E}_e}{\bar{E}_{s1}}\right)}\right]\sqrt{\frac{(\varepsilon_{pre}-\varepsilon_{appl})\varepsilon_c}{1+\varepsilon_{pre}}}, \tag{22}$$

which degenerates to Eq. (16) for a vanishing applied strain on the buckled system without encapsulation layer, i.e., $\varepsilon_{appl}=0$ and $\bar{E}_e=0$. The maximum strain, normalized by its counterpart $\varepsilon_{singlelayer}\approx 2\sqrt{(\varepsilon_{pre}-\varepsilon_{appl})\varepsilon_c/(1+\varepsilon_{pre})}$ for a single-layer substrate without encapsulation, is

$$\frac{\varepsilon_{\max}}{\varepsilon_{singlelayer}}\approx\left(1+\frac{\bar{E}_e}{\bar{E}_{s1}}\right)^{1/3}\left[1+\frac{\left(4\frac{1+\varepsilon_{pre}}{1+\varepsilon_{appl}}\sqrt{\varepsilon_c}\frac{h_s}{h_f}\right)^3e^{-4\frac{1+\varepsilon_{pre}}{1+\varepsilon_{appl}}\sqrt{\varepsilon_c}\frac{h_s}{h_f}\left(1+\frac{\bar{E}_e}{\bar{E}_{s1}}\right)^{1/3}}}{3(1+2r)}\right]. \tag{23}$$

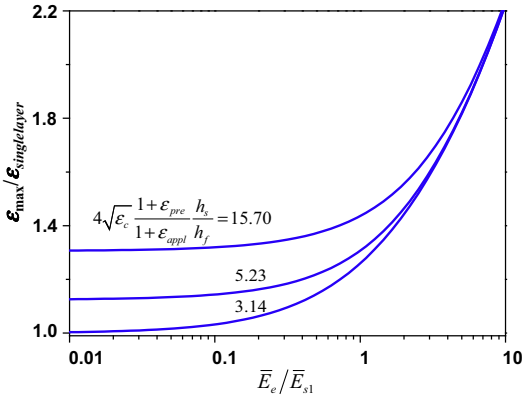

Fig. 5. In the case of encapsulation, the maximum strain $\varepsilon_{\max}$ normalized by its counterpart $2\sqrt{\varepsilon_{pre}\varepsilon_c/(1+\varepsilon_{pre})}$ for a thick, single-layer substrate without encapsulation versus the moduli ratio $\bar{E}_e/\bar{E}_{s1}$ of the encapsulation to top substrate layers for different values of $4h_s(1+\varepsilon_{pre})\sqrt{\varepsilon_c}/[h_f(1+\varepsilon_{appl})]$.

Fig. 5 shows the normalized maximum strain above versus the normalized modulus $\bar{E}_e/\bar{E}_{s1}$ of the encapsulation layer for several values of $4h_s(1+\varepsilon_{pre})\sqrt{\varepsilon_c}/[h_f(1+\varepsilon_{appl})]$ and $r=1/20$. The maximum strain increases with the modulus of the encapsulation layer, which suggests that the system stretchability decreases as the encapsulation layer becomes stiff. For an encapsulation layer as compliant as the top substrate, the maximum strain is 1.26 times of that without encapsulation. This factor of increased is reduced to 1.03 for $\bar{E}_e/\bar{E}_{s1}=0.1$.

5. Concluding remarks

The buckling and post-buckling behaviors for stiff thin films on bi-layer compliant substrates are investigated. The mechanics analysis shows that the top, soft layer of the substrate facilitates buckling to enable stretchability in the intrinsically brittle thin films, whereas the relatively stiff layer at the bottom in the substrate offers robustness and high strength to the system. A soft encapsulation layer can also be used on top of the device for mechanical protection, but the stretchability of the system decreases as the Young's modulus of the encapsulation layer increases. The simple, analytic solution, validated by both the numerical and FEA results, is useful to the design of bi-layer substrates for stretchable electronics.

Acknowledgments

Huanyu Cheng is a Howard Hughes Medical Institute International Student Research fellow. The supports from NSF (DMR-1242240) and NSFC are acknowledged.

References

ABAQUS, 2009. Analysis User's Manual V6.9 (Dassault Systemes, Pawtucket, RI).
Allen, H.G., 1969. Analysis and Design of Structural Sandwich Panels. Pergamon Press, Oxford, vol. 51.
Cao, C. et al., 2013. Harnessing localized ridges for high-aspect-ratio hierarchical patterns with dynamic tunability and multifunctionality. Adv. Mater 26 (11), 1763–1770.
Cheng, H. et al., 2012. An analytical model for shear-enhanced adhesiveless transfer printing. Mech. Res. Commun. 43, 46–49.
Cheng, H., Song, J., 2013. A simply analytic study of buckled thin films on compliant substrates. J. Appl. Mech. 81 (2), 024501.
Duan, Y. et al., 2013. Non-wrinkled, highly stretchable piezoelectric devices by electrohydrodynamic direct-writing. Nanoscale 6, 3289–3295.
Fan, J.A. et al., 2014. Fractal design concepts for stretchable electronics. Nature Communications 5.
García, J.M. et al., 2010. High-performance aromatic polyamides. Prog. Polym. Sci. 35 (5), 623–686.

Huang, Z., Hong, W., Suo, Z., 2005. Nonlinear analyses of wrinkles in a film bonded to a compliant substrate. J. Mech. Phys. Solids 53 (9), 2101–2118.
Hwang, S.-W. et al., 2012. A physically transient form of silicon electronics. Science 337 (6102), 1640–1644.
Jeong, J.-W. et al., 2013. Materials and optimized designs for human-machine interfaces via epidermal electronics. Adv. Mater 25 (47), 6839–6846.
Jiang, H.Q. et al., 2007. Finite deformation mechanics in buckled thin films on compliant supports. Proc. Nat. Acad. Sci. U.S.A. 104 (40), 15607–15612.
Kim, D.H. et al., 2009. Ultrathin silicon circuits with strain-isolation layers and mesh layouts for high-performance electronics on fabric, vinyl, leather, and paper. Adv. Mater. 21 (36), 3703–3707.
Kim, D.H. et al., 2011a. Materials for multifunctional balloon catheters with capabilities in cardiac electrophysiological mapping and ablation therapy. Nat. Mater. 10 (4), 316–323.
Kim, D.-H. et al., 2011b. Epidermal electronics. Science 333 (6044), 838–843.
Kim, S. et al., 2012. Enhanced adhesion with pedestal-shaped elastomeric stamps for transfer printing. Appl. Phys. Lett. 100 (17), 171909.
Ko, H.C. et al., 2008. A hemispherical electronic eye camera based on compressible silicon optoelectronics. Nature 454 (7205), 748–753.
Li, R. et al., 2013. An analytical model of reactive diffusion for transient electronics. Adv. Funct. Mater 23 (24), 3106–3114.
Lu, N. et al., 2007. Metal films on polymer substrates stretched beyond 50%. Appl. Phys. Lett. 91 (22), 221909.
Lu, N. et al., 2012. Highly sensitive skin-mountable strain gauges based entirely on elastomers. Adv. Funct. Mater. 22 (19), 4044–4050.
Song, J. et al., 2008. Buckling of a stiff thin film on a compliant substrate in large deformation. Int. J. Solids Struct. 45 (10), 3107–3121.
Song, Z. et al., 2014. Origami lithium-ion batteries. Nat. Commun. 5.
Timoshenko, S.P., Goodier, J., 2011. Theory of elasticity. Int. J. Bulk Solids Storage Silos 1 (4), 567.
Wang, Q., Zhao, X., 2014. Phase diagrams of instabilities in compressed film-substrate systems. J. Appl. Mech. 81 (5), 051004.
Webb, R.C. et al., 2013. Ultrathin conformal devices for precise and continuous thermal characterization of human skin. Nat. Mater. 12 (10), 938–944.
Xiao, J.L. et al., 2009. Alignment controlled growth of single-walled carbon nanotubes on quartz substrates. Nano Lett. 9 (12), 4311–4319.
Xiao, J. et al., 2010. Analytical and experimental studies of the mechanics of deformation in a solid with a wavy surface profile. J. Appl. Mech.-Trans. ASME 77 (1), 011003.
Xu, S. et al., 2013. Stretchable batteries with self-similar serpentine interconnects and integrated wireless recharging systems. Nat. Commun. 4, 1543.
Yang, S.Y. et al., 2012. Elastomer surfaces with directionally dependent adhesion strength and their use in transfer printing with continuous roll-to-roll applications. Adv. Mater. 24, 2117–2122.
Zang, J. et al., 2013. Multifunctionality and control of the crumpling and unfolding of large-area graphene. Nat. Mater. 12 (4), 321–325.